Nuclear Instruments and Methods in Physics Research A 763 (2014) 6–12

Contents lists available at ScienceDirect

Nuclear Instruments and Methods in Physics Research A

journal homepage: www.elsevier.com/locate/nima

Design study of an ultra-compact superconducting cyclotron for isotope production

V. Smirnov [a,*], S. Vorozhtsov [a], J. Vincent [b]

[a] Joint Institute for Nuclear Research, Dubna, Russia
[b] Ionetix Corporation, Lansing, MI 48911, USA

ARTICLE INFO

Article history:
Received 23 March 2014
Received in revised form
2 June 2014
Accepted 3 June 2014
Available online 12 June 2014

Keywords:
Cyclotron
Superconductivity
Computer simulation
Beam dynamics
Electromagnetic fields
Medical isotope

ABSTRACT

A 12.5 MeV, 25 μA, proton compact superconducting cyclotron for medical isotope production has been designed and is currently in fabrication. The machine is initially aimed at producing ^{13}N ammonia for Positron Emission Tomography (PET) cardiology applications. With an ultra-compact size and cost-effective price point, this system will offer clinicians unprecedented access to the preferred radio-pharmaceutical isotope for cardiac PET imaging. A systems approach that carefully balanced the subsystem requirements coupled to precise beam dynamics calculations was followed. The system is designed to irradiate a liquid target internal to the cyclotron and to minimize the need for radiation shielding. The main parameters of the cyclotron, its design, and principal steps of the development work are presented here.

1. Introduction

A 12.5 MeV, 25 μA, proton compact superconducting cyclotron for medical isotope production has been designed and is currently in fabrication. The machine is initially aimed at producing ^{13}N ammonia for myocardial perfusion positron emission tomography (PET) studies applied to the detection of coronary artery disease. The "ION-12SC" [1] cyclotron features a cryogen free magnet small enough to operate within a standard medical space similar to that utilized by a typical PET scanner.^{13}N ammonia is produced in a liquid target internal to the cyclotron. Usability, reliability and compact size with a cost-effective price are the key requirements of the design.

To allow for efficient mass production, installation and operation by a trained non-technical staff, the cyclotron design and operation must be kept simple. To provide for high reliability and operating efficiency, the requirements for each subsystem must be kept modest and well within physical limits. The machine design philosophy has to be one of robustness optimizing low sensitivity to perturbations versus high performance. The basic design arrived at achieved the following key points.

- To keep the machine size small and simple, a compact cryogen-free superconducting magnet featuring a patented cold steel design was applied such that the magnetic yoke is in thermal contact with the superconducting coils [2].
- The final energy radius of 115 mm was arrived at as a qualitative compromise between machine size and required peak RF voltages.
- The RF system consists of a simple conventional ~175° dee operating in the 1st harmonic mode and applying a peak voltage of ≤ 20 kV.
- The ion source consists of a cold cathode PIG source that is positioned to center the starting beam.
- Beam quality such as brightness and timing is not an issue for this application.
- No extraction system is needed since an internal target will be used. Some turn separation is needed to minimise losses on the target window frame.

The conceptual design is shown in Fig. 1.

State of the art detailed 3D calculations were performed. The electromagnetic fields of the structural elements were calculated using the Tosca\Opera3D program [3]. The SNOP program [4] was used to determine particle tracing in the in full 3D fields of the magnet and RF system. The main parameters of the cyclotron are listed in Table 1.

2. Magnetic system

The magnet design must set the average field profile to maintain isochronism and provide the required flutter to maintain

* Corresponding author. Tel.: +74962162160; fax: +74962166666.
E-mail address: vsmirnov@jinr.ru (V. Smirnov).

http://dx.doi.org/10.1016/j.nima.2014.06.013
0168-9002/

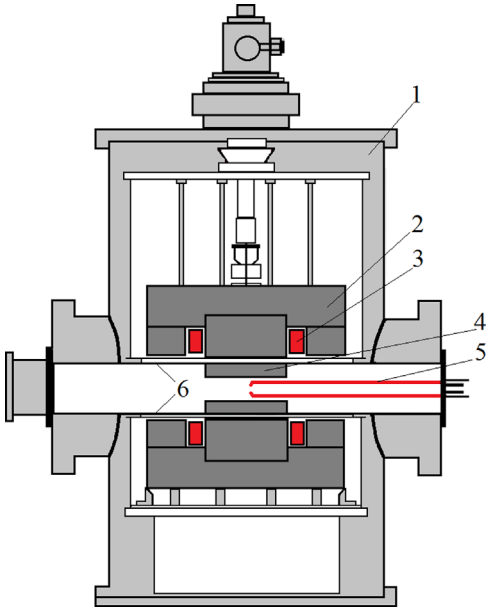

Fig. 1. Schematic presentation of the magnet structure (not to scale): 1—outer cryostat, 2—yoke, 3—superconducting coil, 4—warm spiral poles, 5—dee, 6—warm bore.

Table 1
Main cyclotron parameters.

Parameter	Value
Cyclotron type	Compact, Isochronous
Accelerated particle	Proton
Injection type	Internal PIG source
Central magnetic field	4.5 T
RF system	Single 175° dee
Operation RF harmonic	1
RF frequency	68 MHz
Peak dee voltage	≤20 kV
Final energy	12.5 MeV
Beam intensity	>25 μA
Final radius	115 mm
Cyclotron diameter	870 mm
Cyclotron height	1253 mm
Cyclotron weight	1570 kg
Magnet (iron+coils) weight	900 kg

focus. The design requirements resulted in the following criteria and conditions.

- A warm bore through the magnet provides the mounting surfaces for the warm iron sectored poles and must maintain a minimum 30 mm vertical gap to accommodate the ion source, RF resonator, internal target, and other equipment as is needed (see Fig. 1).
- There must be a minimum of 17 mm thermodynamic barrier between the outer surfaces of the warm bore and sectored poles to the cold steel.
- The cold steel yoke is to be manufactured of AISI 1008 steel.
- The SC coils are wet wound with Ecobond 24 resin using Supercon NbTi 54S43 1 mm insulated diameter wire.
- The coil current density is limited to 150 A/mm^2 to reduce the forces and coil fields to conservative values for the wire specified.
- A 1.5 W cryocooler is used to bring the coil temperatures below 4.5 K through proprietary linkages.
- The vertical coil forces are consistently directed away from the median plane into and supported by the surrounding magnet yoke and vary from a high value of ~140 kN during the ramp to the operating value of 20 kN.
- The force on the warm iron poles is ~20 kN directed away from the cyclotron median plane.

The *B–H* curve of the magnet yoke was modeled as steel-08 produced by the Izhora factory in St. Petersburg, Russia. The *B–H* curve for this steel was measured by CERN in Switzerland up to 1.96 T for the CMS experiment (LHC, CERN) [5]. This curve was reasonably

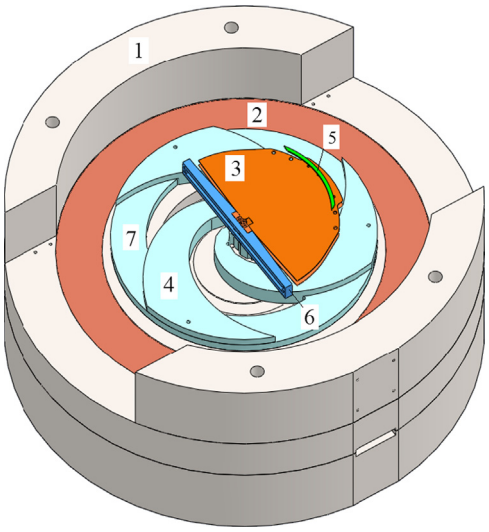

Fig. 2. Cyclotron mechanical model: 1—yoke, 2—superconducting coil, 3—dee, 4—spiral shim, 5–1st harmonic shim, 6—dummy dee, 7—valley shim.

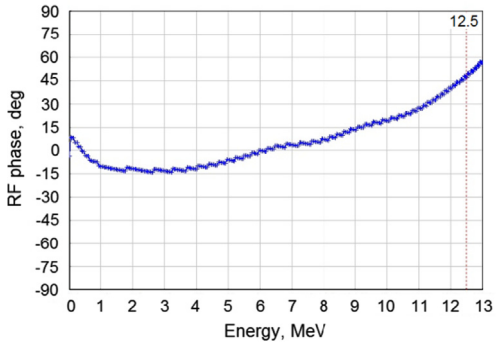

Fig. 3. Beam RF phase excursion.

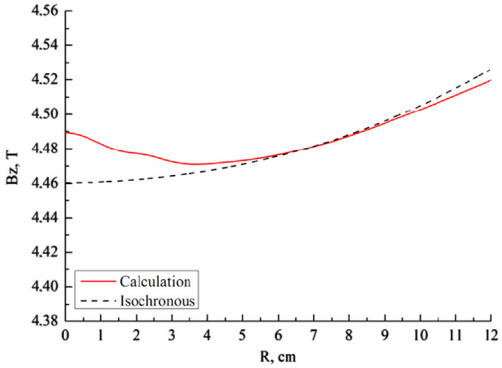

Fig. 4. Mean magnetic field vs. radius.

extrapolation to higher fields and the steel properties are known to be close to standard AISI 1010 steel. As is typical in superconducting magnets, the magnetic field is a combination of that provided by the saturated iron and the coils. In our case, approximately 60% of the field is provided by the coils. To facilitate rapid trial and error runs of these nonlinear cases, the 3D magnetic model was approximated by a 2.5D model replacing the spiral poles with circularly symmetric equivalent reluctance disks. This method was used to shape the field and to crosscheck the sophisticated 3D field simulations by the Tosca VF code.

Achieving an acceptable field shape with the imposed requirements was a difficult task. The median plane top view of the magnetic structure is shown in Fig. 2.

The magnet requirements were satisfied in the following ways.

- The superconducting coils are epoxy wound with no cooling holes.
- To aid in field shaping and reduce the need for shimming, the warm iron spiral sectored poles are manufactured of Armco pure iron.
- The large axial gap between the saturated sectors severely limits the flutter. To provide for sufficient axial beam focusing, the main magnetic field is formed by a minimal set of three logarithmical spiral sectors with a 60° angle.
- The necessary increase in the magnetic field needed to maintain the isochronous condition was carefully balanced against the minimal focusing available.
- To obtain the needed radial magnetic field shape to support isochronism, iron was added to the valleys between the 60° spiral poles near the final radius.

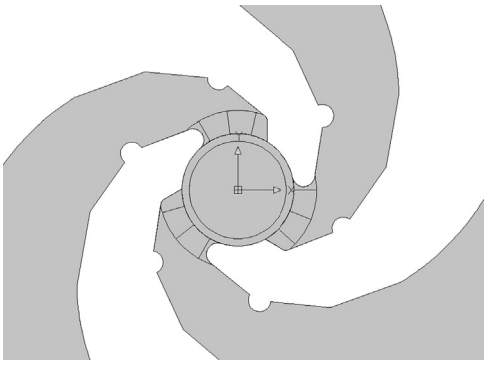

Fig. 5. Structure of the spiral sectors in the central region.

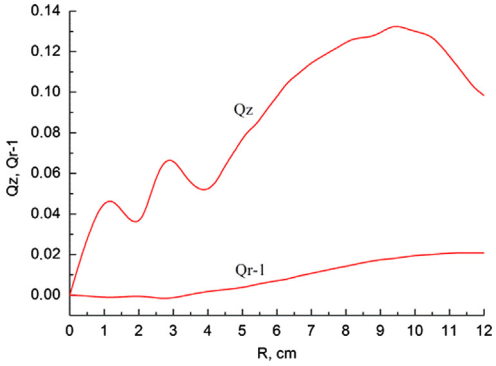

Fig. 6. Betatron tunes.

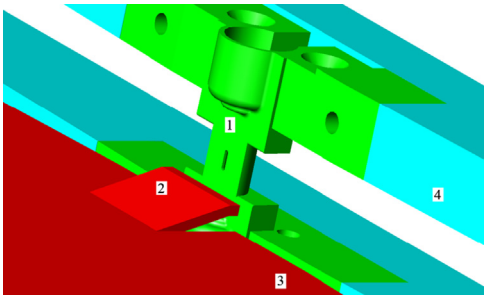

Fig. 7. Central region structure: 1—ion source, 2—puller, 3—dee, 4—dummy dee.

With a coil excitation of 680 kA-turns/pole, the resulting mean field dependence with radius and the field index was slightly below that of the isochronous curve. This results in the *RF* phases of the particles slipping to near 50° at the final energy (see Fig. 3). Acceleration in this field leads to an increased number of turns, but keeps the geometrical dimensions of the accelerator moderate.

To somewhat boost the axial focusing of the beam in the machine center where the flutter is very small, the central plug was shaped to provide a decreasing mean magnetic field to a radius of about 4 cm (Fig. 4).

It is well known that the flutter magnitude decreases with increase of the spiral angle. For some cyclotrons with a large enough magnetic field, this property becomes critical in the central region of the accelerator. The effective spiral angle in the center of the cyclotron decreases resulting in a degradation of the flutter there. To boost the flutter value in the central region and keep the spiral angle intact or decreased only slightly, the spiral sector is composed of piece-wise radial sectors approaching the theoretical spiral shape [6] (Fig. 5). This result in combination with the additional focusing by the RF electric field provided stable axial motion of the beam in the initial turns.

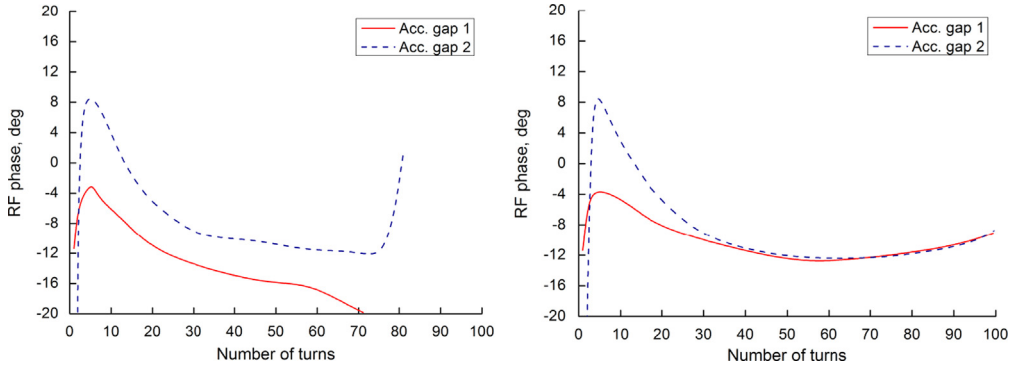

Fig. 8. Example of RF phase excursion for a particle dropped from acceleration (left side, initial RF phase −15°) and for a particle captured to the acceleration (right side, initial RF phase 0°).

An analysis of betatron frequencies (Fig. 6) with the resulting field shape shows that an introduction of the magnetic bump in the central region substantially contributes to the axial focusing there.

The midplane radial bore through the magnet yoke needed to accommodate the warm bore (Fig. 2) introduces a 2nd harmonic field component of 0–25 Gs amplitude. It increases approximately linearly with radius from the central region to the final radius. The beam simulation shows that it just slightly changes the transmission (relative reduction ~10%) and the beam quality at the final radius. This can be reduced through compensation if needed.

3. Acceleration system

The RF resonator fits between the spiral pole faces that are spaced 30 mm apart at the operating magnetic field. 1 mm of space is allotted for clearance between the RF resonator box and the pole surfaces. The RF box outer conductor plates and dee plates are 1 mm thick and the dee plates are spaced 10 mm apart. This results in a clearance between the dee plates and the inner box surfaces of 7 mm. The resulting capacitance of the dee, operating voltage, and associated stem drives the conduction currents resulting in the resonator conduction losses. Although the beam dynamics would prefer the poles be spaced closer together and a higher operating dee voltage, this was weighed carefully against the resulting increased RF losses to arrive at this design.

The model of the structure described along with the central region design was used to determine the electrical field distributions used in the beam dynamics analysis. The elements of the RF resonator – dee and dummy dee – affecting the beam dynamics calculations are visible in the mechanical model of the machine, see Fig. 2.

4. Central region

The simplest central region that would provide the needed stable beam generation and capture was sought. A PIG type ion source with an internal chimney radius of 1 mm generates the needed proton beam. An ion source test stand with a 0.25 T applied magnetic field was used to experimentally determine a suitable ion source opening slit of 0.5×2 mm^2. The source was found to operate at ~800 VDC and 1 mA for a total output current of 100 μA. Significantly higher output currents were readily available to achieve the needed cyclotron performance. The source efficiency is expected to improve somewhat at the operating field of ~4.5 T. For example, the IBA S2C2 synchrocyclotron PIG cold cathode ion source with 5.7 T central magnetic field [7] works well in this environment.

In the very center of the machine, the axial gap of the dee is reduced from 10 to 5 mm to provide an effective puller (Fig. 7).

The gap between the dee and the dummy dee is 1.5 mm and the dee voltage is 20 kV. With 68 MHz we have about 1.3 Kilpatrick

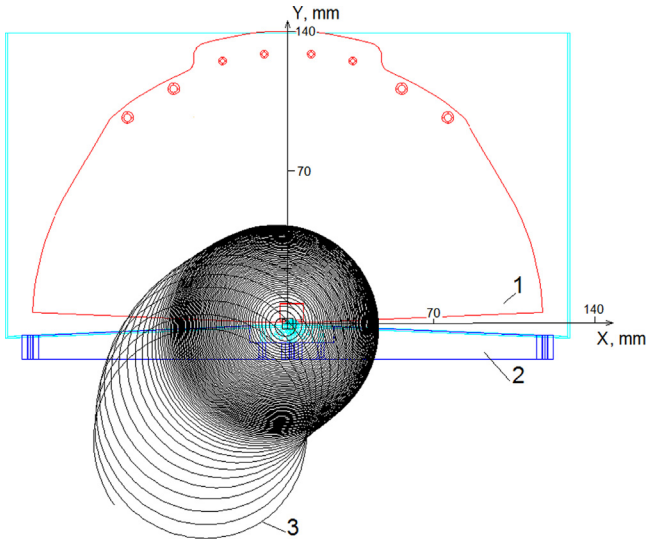

Fig. 9. Trajectory of particle decentered and lost on the vacuum chamber walls. Particle initial RF phase −15°. Ion source is located on the *Y* axis. 1—dee, 2—dummy dee, 3—particle trajectory.

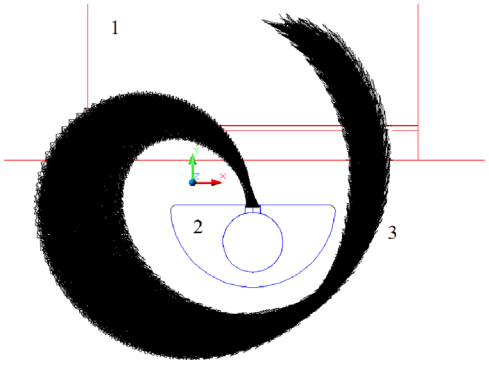

Fig. 11. Bunch of particles captured in the acceleration: 1—puller, 2—ion source, 3—particle trajectories.

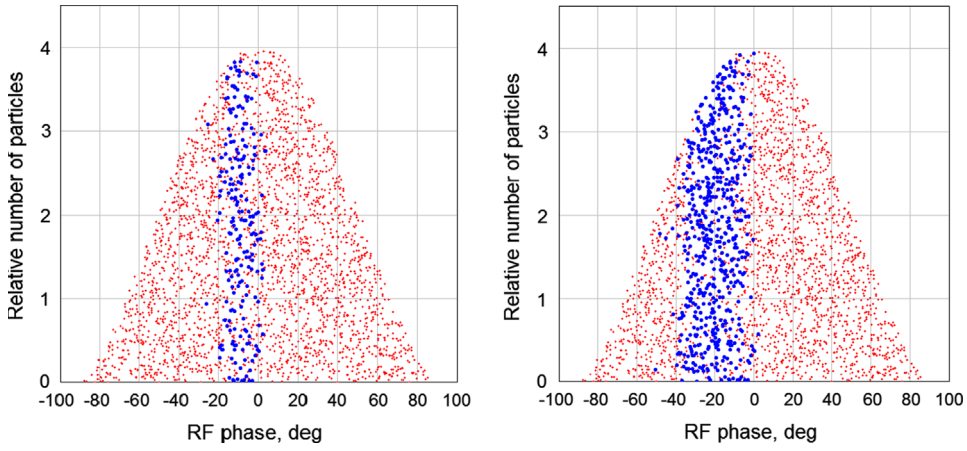

Fig. 10. Phase acceptance for initial (left) and for optimal (right) position of the ion source. In the figure each dot symbolically represents an emitting particle with the total number of particles in the given RF phase range obeying the Child's law.

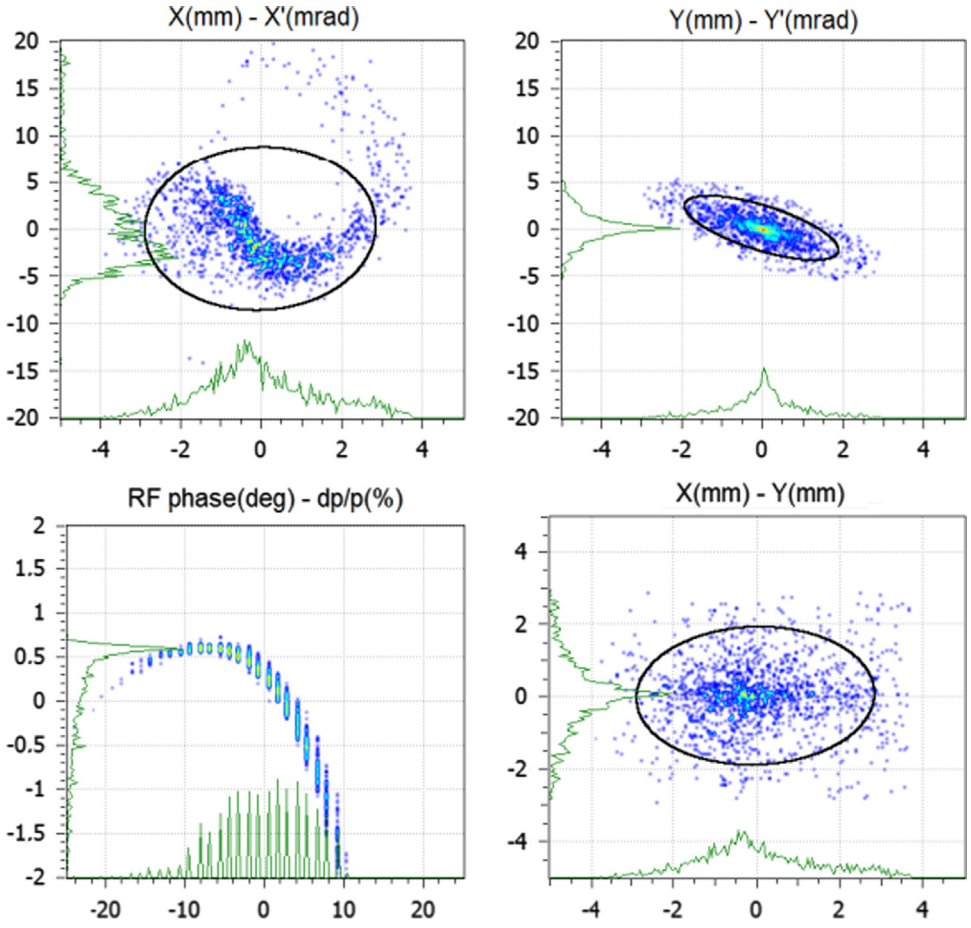

Fig. 12. Beam emittances at the final radius in a coordinate system centered on the bunch. *X*—horizontal transverse axis, *Y*—vertical transverse axis.

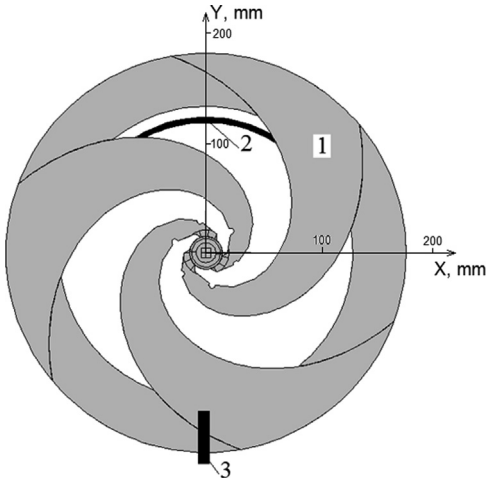

Fig. 13. First harmonic introduction: 1—magnet sector, 2–1st harmonic shim, 3—target location.

sparking probability (1 Kilpatrick equals to ~100 kV/cm at this frequency).

The optimization of the central region structure was based on calculations of the efficiency of the beam transmission starting from the ion source and ending on the final radius. The accelerator acceptance was also estimated at this time. The calculations were preformed with bunch which utilizes 50,000 macro-particles and takes spaces charge forces into account. The SNOP program provides space charge calculations by the PIC (Particle-In-Cell) method using a FFT (Fast Fourier Transform) to solve the Poisson's equation. Some optimization of the number of the knots in the FFT grid was also made. However, since the beam current in this machine is less than 30 μA, space charge forces are not a concern.

The initial beam distribution vs. starting RF phase at the output slit of the ion source used in the simulations is shown in Fig. 10 (red dots in the phase range ±90°). The instantaneously available current from the ion source increases with applied extraction (Dee) voltage. To a first approximation, we assume that the shape of the chart in Fig. 10 follows the Child's (or three-halves-power) law [8] that gives the maximum space-charge-limited current in a planar diode of infinite radius as a function of the length and potential difference between anode and cathode. Consistent with information commonly available [9], the initial particle energy at the ion source output slit is assumed to be some very low value of approximately 5 eV. The initial particle distribution emanating from the ion source is assumed to be a uniform distribution filling the area of the ion source slit. The assumed transverse phase space at the ion source output was formed with uniform particle density within elliptic boundaries defining emittances of ~1.3π mm mrad [9]. The value of initial angular spread from the source assumed is of little consequence since after crossing the first acceleration gap the low initial energy is completely overwhelmed by the RF acceleration thus completely redefining the angular spread.

The original location of the ion source was at the dee symmetry axis. In this location, the calculated transmission in the initial turn was ~25% with only about 5% surviving to full energy. The losses are explained by less than ideal starting conditions leading to large and growing de-centering of the beam due to the RF phase imbalance as plotted in (Fig. 8, left). On the contrary, the particles

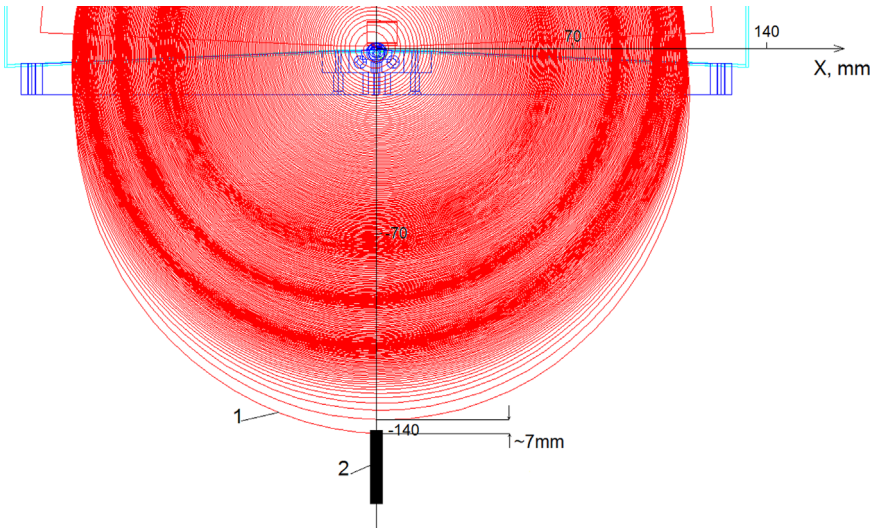

Fig. 14. Reference orbits in the magnetic field with the 1st harmonic near the final radius: 1—reference trajectory, 2—target.

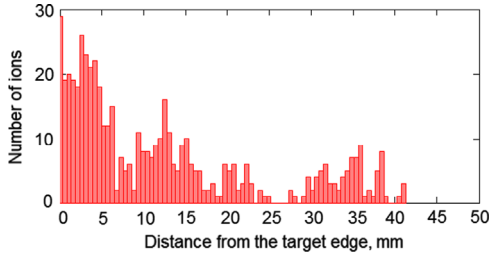

Fig. 15. Particle distribution on the target. It is assumed that the target area begins at 0 mm in the horizontal axis. The other edge of the target is not shown since it will be defined after completion of its design. The vertical axis shows the number of particles intercepted by the target at a given radial position defined in the horizontal axis. The multi-turn extraction takes place.

captured in acceleration do not have such a large RF phase difference as plotted in (Fig. 8, right). In the figure the RF phases along the acceleration gap are depicted. The initial RF phase corresponds to the position of the emitting particle at the slit of the ion source. In these calculations, the same location of the ion source was assumed in both parts of the figure. In the first several turns, a visible difference in the RF phase performance with turn number exists that is based on the RF starting phases and continues to grow downstream.

The motion of the majority of the particles is similar to acceleration with different effective dee voltages at the dee gaps. This is reminiscent of particle motion in a magnetic field containing the 1st harmonic. As a result, the particles affected are either lost or acquire much smaller energy at the final radius than the nominal ones (Fig. 9).

The method chosen to center the beam adjusts the ion source off center an optimal distance. The calculations show that the optimal location of the ion source is 2 mm off the dee symmetry axis along the dee to dummy dee gap. This increased the transmission from ion source slit to the final radius from 5 to 21%. With an ion source proton current of ~500 μA in DC tests this results in 25 μA at full energy. The RF acceptance angle increased by ~2 times and the population density of the particles substantially increases in this phase range (Fig. 10). An attempt to find the minimum possible voltage necessary for stable acceleration to full energy shows that at the peak dee voltage of 16 kV we lose 50% of the maximal beam.

The analysis of the particle motion for the initial turns shows nearly all particles with starting phases between -40° to 0° are accepted. Fig. 11 shows the trajectories of the particles that are successfully captured into the acceleration regime. The probability for a particle to reach the final radius is mostly defined by its initial RF phase, although there is some dependence on the particle initial position within the slit of the ion source. As mentioned previously, the particle emitting angle has practically no effect on its capture since the ion trajectory in the 1st acceleration gap is predominantly defined by the electrical field distribution.

The axial losses of the particles during acceleration is nearly zero since the ion source slit axial size (2 mm) is noticeably smaller than the axial aperture of the RF system (10 mm) in combination with the previously described axial focusing from both the RF electric field and the central magnetic bump.

5. Production target

An internal proprietary liquid target featuring a frameless metal foil window currently in development will be installed near the final radius of the cyclotron for ^{13}N isotope generation. The target will contain ~3 ml of O16 water over pressurized with methane which is a common practice for production of N13 ammonia. Turn separation at this radius is required to minimize losses on the target window. The horizontal size of the beam at this location is ~6 mm ($2\times 2\sigma$, Fig. 12). A magnetic 1st harmonic near the final radius has been designed to off-center the beam and provide turn separation (Fig. 13). The goal was to get greater than 80% of the particles into the active target region. The passive magnetic 1st harmonic added in combination with the dropping main magnetic field provided reasonable turn separation.

The maximal turn separation occurs 180° downstream from the added static valley shim with 5 mm × 2.3 mm cross-section (Fig. 14). A movable target in the dummy dee side of the beam chamber will help to optimize the amount of beam intercepted by the active region of the target.

The introduction of the 1st magnetic harmonic near the final energy radius leads to dilution of the particle density along the radius in the region under consideration, i.e., a number of particles in the given radial range decreases with the 1st harmonic amplitude. Therefore, the resulting losses on the target frame should reduce as well. Calculations show that a 40 Gs amplitude 1st harmonic near the final radius increases the particle turn separation to ~7 mm (Fig. 14), and the losses becomes ~10% for the radial position of the target frame R_{target} ~140 mm with

internal frame 1 mm (Fig. 15). So, ~90% of the beam can be used for ^{13}N production in compliance with the requirements formulated above.

6. Summary

Computer simulations of the cyclotron (magnet, beam dynamics, acceleration system) have been completed. Engineering is nearing completion and detailed mechanical drawings of the systems have been prepared.

The magnet is under construction and the warm bore has been engineered and manufactured. A proton cold cathode source and associated test stand have been assembled and have been actively used for some time measuring the performance and lifetime parameters. The slit size described was determined during these tests.

Upon completion, the magnet will be integrated with the rest of the systems (RF, ion source, beam probe, target, controls and instrumentation, etc.) and beam testing is planned to begin immediately thereafter.

References

[1] K.J. Cameron, The Revolutionary ION-12SC for N-13 Ammonia Production, The Society of Nuclear Medicine Molecular Imaging 2013 Annual Meeting. Ionetix Corporation (Booth 544), Vancouver, BC, 2013.
[2] Compact, Cold, superconducting isochronous cyclotron, Patent number: US8558485B2, Assignee: Ionetix Corporation.
[3] Cobham CTS Ltd Vector Fields Software. United Kingdom: Network House, Langford Locks, Kidlington, Oxfordshire, OX5 1LH.
[4] V.L. Smirnov, S.B. Vorozhtsov, SNOP—beam dynamics analysis code for compact cyclotrons, in: Proc. of the XXI Russian Accelerator Conference, RuPAC'2012, St. Petersburg, Russia, 2012.
[5] V.I. Klioukhine, D. Campi, B. Curé, A. Desirelli, S. Farinon, H. Gerwiget al, IEEE Trans. Appl. Supercond. 10 (1) (Mar. 2000) 428.
[6] S. A. Artamonov, E. M. Ivanov, G. A. Riabov, N. A. Chernov, Highly accurate 3D modeling of the C-80 isochronous cyclotron magnetic structure, in: Proceedings of RUPAC2012, Saint-Petersburg, Russia.
[7] W. Kleeven et al. The IBA superconducting synchrocyclotron project S2C2. MO4PB02, in: Proc. of the Int. Conference Cyclotrons'13, Vancouver, BC, Canada.
[8] C. D. Child, Phys. Rev. Series I 32 (5): 492.
[9] E. R. Forringer, Phase Space Characterization of an Internal Ion Source for Cyclotrons, PhD Dissertation, MSU. 2004.